Optics

The focusing optics consists of two parts, which first focus and then re-collimate the beam for diagnostic purposes (see Fig. 1). Both parts have a numerical aperture of 0.7, a working distance of 1 cm, and a common focal point set at the centre of the MOT. The focusing objective consists of nine lenses, and achieves a diffraction-limited resolution of 0.7 μm, while the re-collimating objective consists of four lenses. The fluorescence light induced by the MOT beams is collected by the focusing objective, and gives a magnified image of the trap on a CCD camera. As the CCD camera has a slow response time, an APD is used in parallel, and monitors only the light coming from the trap region. Typically, the 1-μm-diameter dipole trap is imaged onto a 50-μm pinhole with a magnification of 20. The pulses from the APD are continuously registered by a computer, and can be processed to get histograms, intensity correlations, or photon counting statistics within the counting window.

Dipole trap

The linearly polarized dipole trap beam from a frequency stabilized titanium–sapphire laser is brought to the set-up using an optical fibre. Its wavelength is 810 nm, to be compared with the 795 nm (D1) and 780 nm (D2) lines of rubidium, so the trap operates far off resonance[22], where the spontaneous emission is very small. The typical oscillation frequency in the trap along the x–y (transverse) axes is calculated to be close to 200 kHz; this value has been confirmed experimentally by using parametric excitation of the oscillatory motion. The MOT cooling is expected to be working over a significant fraction of the potential well of the dipole trap. The trapped-atom temperature can be evaluated by measuring the fluorescence decay when turning off the MOT and dipole trap beams, and after some time turning on the MOT again. Data from the present experimental set-up, which is being improved, show that the trapped atom temperature is higher than 50 μK. An upper limit is given by the smallest potential for reliably trapping one atom, which is at present 1 mK. More accurate measurements of the temperature and motional properties of the trapped atom are under way.

Received 14 March; accepted 11 May 2001.

1. Sackett, C. A. *et al.* Experimental entanglement of four particles. *Nature* **404,** 256–259 (2000).
2. Steane, A. *et al.* Speed of ion-trap quantum-information processors. *Phys. Rev. A* **62,** 042305-1–042305-9 (2000).
3. Walther, H. Single atom experiments in cavities and trap. *Proc. R. Soc. Lond. A* **454,** 431–445 (1998).
4. Rauschenbeutel, A. *et al.* Coherent operation of a tunable quantum phase gate in cavity QED. *Phys. Rev. Lett.* **83,** 5166–5169 (1999).
5. Calarco, T., Briegel, H. J., Jaksch, D., Cirac, J. I. & Zoller, P. Entangling neutral atoms for quantum information processing. *J. Mod. Opt.* **47,** 2137–2149 (2000).
6. Brennen, G. K., Deutsch, I. H. & Jessen, P. S. Entangling dipole-dipole interactions for quantum logic with neutral atoms. *Phys. Rev. A* **61,** 062309-1–062309-10 (2000).
7. Morinaga, M., Bouchoule, I., Karam, J. C. & Salomon, C. Manipulation of motional quantum states of neutral atoms. *Phys. Rev. Lett.* **83,** 4037–4040 (1999).
8. Doherty, A. C., Lynn, T. W., Hood, C. J. & Kimble, H. J. Trapping of single atoms with single photons in cavity QED. *Phys. Rev. A* **63,** 013401-1–013401-24 (2001).
9. Pinkse, P. W. H., Fischer, T., Maunz, P. & Rempe, G. Trapping an atom with single photons. *Nature* **404,** 365–368 (2000).
10. Hu, Z. & Kimble, H. J. Observation of a single atom in a magneto-optical trap. *Opt. Lett.* **19,** 1888–1890 (1994).
11. Ruschewitz, F., Bettermann, D., Peng, J. L. & Ertmer, W. Statistical investigations on single trapped neutral atoms. *Europhys. Lett.* **34,** 651–656 (1996).
12. Frese, D. *et al.* Single atoms in an optical dipole trap: towards a deterministic source of cold atoms. *Phys. Rev. Lett.* **85,** 3777–3780 (2000).
13. Calarco, T. *et al.* Quantum gates with neutral atoms: Controlling collisional interactions in time-dependent traps. *Phys. Rev. A* **61,** 022304-1–022304-11 (2000).
14. Brennen, G. K., Caves, C. M., Jessen, P. S. & Deutsch, I. H. Quantum logic gates in optical lattices. *Phys. Rev. Lett.* **82,** 1060–1063 (1999).
15. DePue, M. T. *et al.* Unity occupation of sites in a 3D optical lattice. *Phys. Rev. Lett.* **82,** 2262–2265 (1999).
16. Rempe, G. & Walther, H. Sub-Poissonian atomic statistics in a micromaser. *Phys. Rev. A* **42,** 1650–1655 (1990).
17. Orzel, C., Tuchman, A. K., Fenselau, M. L., Yasuda, M. & Kasevich, M. A. Squeezed states in a Bose-Einstein condensate. *Science* **291,** 2386–2389 (2001).
18. Gensemer, S. D., Gould, P. L., Leo, P. J., Tiesinga, E. & Williams, C. J. Ultracold ^{87}Rb ground-state hyperfine-changing collisions in the presence and absence of laser light. *Phys. Rev. A* **62,** 030702-1–030702-4 (2000).
19. Nesnidal, R. C. & Walker, T. G. Light-induced ultracold spin-exchange collisions. *Phys. Rev. A* **62,** 030701-1–030701-4 (2000).
20. Kuppens, S. J. M., Corwin, K. L., Miller, K. W., Chupp, T. E. & Wieman, C. E. Loading an optical dipole trap. *Phys. Rev. A* **62,** 013406-1–013406-13 (2000).
21. Jaksch, D. *et al.* Fast quantum gates for neutral atoms. *Phys. Rev. Lett.* **85,** 2208–2211 (2000).
22. Miller, J. D., Cline, R. A. & Heinzen, D. J. Far-off-resonance optical trapping of atoms. *Phys. Rev. A* **47,** R4567– R4570 (1993).

Acknowledgements

The contributions of K. Vigneron, H. Wilhelm and T. Zhang to early stages of the experiment are acknowledged. This work was supported by the European IST/FET programme 'QUBITS' and by the European IHP network 'QUEST'.

Correspondence and requests for materials should be addressed to P.G. (e-mail: philippe.grangier@iota.u-psud.fr).

Nonlinear limits to the information capacity of optical fibre communications

Partha P. Mitra & Jason B. Stark

Bell Laboratories, Lucent Technologies, Murray Hill, New Jersey 07974, USA

The exponential growth in the rate at which information can be communicated through an optical fibre is a key element in the 'information revolution'. However, as for all exponential growth laws, physical limits must be considered. The nonlinear nature of the propagation of light in optical fibre has made these limits difficult to elucidate. Here we use a key simplification to investigate the theoretical limits to the information capacity of an optical fibre arising from these nonlinearities. The success of our approach lies in relating the nonlinear channel to a linear channel with multiplicative noise, for which we are able to obtain analytical results. In fundamental distinction to linear channels with additive noise, the capacity of a nonlinear channel does not grow indefinitely with increasing signal power, but has a maximal value. The ideas presented here may have broader implications for other nonlinear information channels, such as those involved in sensory transduction in neurobiology. These have been often examined using additive noise linear channel models[1] but, as we show here, nonlinearities can change the picture qualitatively.

The classical theory of communications[1] was developed mostly in the context of linear channels with additive noise, which was adequate for electromagnetic propagation through wires and cables that have until recently been the main conduits for information flow. Fading channels or channels with multiplicative noise have been considered, for example in the context of wireless communications[2], although such channels remain theoretically less tractable than the additive noise channels. However, with the advent of optical fibre communications we are faced with a nonlinear propagation channel that poses major challenges to our understanding. The difficulty is that the input–output relationship of an optical fibre channel is obtained by integrating a nonlinear partial differential equation and may not be represented by an instantaneous nonlinearity. Channels where the nonlinearities in the input–output relationship are not instantaneous are in general ill understood, the optical fibre simply being a case of current relevance. The understanding of such nonlinear channels with memory are of fundamental interest, both because communication rates through optical fibre are increasing exponentially and we need to know where the limits are, and also because understanding such channels may give us insight elsewhere, such as into the design principles of neurobiological information channels at the sensory periphery.

The capacity of a communication channel is the maximal rate at which information may be transferred through the channel without error. The capacity can be written as a product of two conceptually distinct quantities, the spectral bandwidth W and the maximal spectral efficiency which we will denote C'. In the classic capacity formula for the additive white gaussian noise channel with an average power constraint, $C = W \log_2(1 + S/N)$, the spectral bandwidth W, which has dimensions of inverse time, multiplies the dimensionless maximal spectral efficiency $C' = \log_2(1 + S/N)$ (sometimes written with 'units' of bits s^{-1} Hz^{-1}). Here S and N are the signal and noise powers respectively. As the maximal spectral efficiency is logarithmic in the signal to noise ratio (S/N), the capacity is principally determined by the bandwidth W. In the case of an optical fibre, the intrinsic loss mechanisms of light propagating

through silica fundamentally limits W to a maximum of about 50 THz (ref. 3) corresponding to a wavelength range of about 400 nm (1.2–1.6 μm). This is to be compared with current systems where the total bandwidth is limited to about 15 THz. If the channel was linear, the maximal spectral efficiency would be $C' = \log_2(1 + S/N)$, S being input light intensity and N the intensity of amplified spontaneous emission noise in the system. An output S/N of say 100 (that is, 20 dB), would then yield a spectral efficiency of 6.6, which for a 50 THz channel would correspond to a capacity of 330 Tbit s^{-1}. The channel, of course, is not linear; so how do the nonlinearities affect the spectral efficiency of the fibre? Our basic conclusion here is that the impact is severe and qualitative. As shown in Fig. 1, the effect is a saturation and eventual decline of spectral efficiency as a function of input signal power, in complete contrast with the linear channel case. We now proceed to discuss this result.

We concentrate on the most important propagation nonlinearity, namely the intensity dependence of the refractive index[4] n: $n = n_0 + n_2 I$. Here n_0 is the linear refractive index and n_2 is a constant. The nonlinearity is weak, but its effects accumulate over long propagation distances. Three principal parameters are of interest: the group velocity dispersion $\beta \approx 10\,\mathrm{ps^2\,km^{-1}}$, the propagation loss $\alpha \approx 0.2\,\mathrm{dB\,km^{-1}}$ and the strength of the nonlinear refractive index, $\gamma \approx 1\,\mathrm{W^{-1}\,km^{-1}}$. The propagation loss is compensated by interposing optical amplifiers into the system, which inject spontaneous emission noise into the system with strength[5] $I_1 = aGh\nu B$. Here G is the amplifier gain, h is Planck's constant, ν and B are the centre frequency and bandwidth respectively, and a is a numerical constant (which we assume to be 2). For n_s spans of fibre with interspersed amplifiers, absorption may be accounted for by considering an effective length, $L_{\mathrm{eff}} \approx n_s/\alpha$. In the absence of nonlinearity, the maximal spectral efficiency is $C'_0 = \log_2(1 + I/I_n)$, I being the input power and $I_n = n_s I_1$ being the total additive noise power. We note that C'_0 vanishes as the inverse power of the system length.

For a variety of reasons, principally limitations in the electronic bandwidth, it is impractical to modulate the full optical bandwidth at once. Current attempts towards achieving maximal information throughput involve wavelength division multiplexing (WDM), where the whole optical bandwidth is broken up into disjoint frequency bands each of which is modulated separately. We confine our attention to such systems (which from an information theory perspective corresponds to the 'multi-user' case)[6], although we also comment on the ideal case of a single data stream (the 'single-user' case).

The nonlinear propagation effects in the evolution of the electric field amplitude involve a cubic term in the electric field. In a WDM system, the nonlinearities are classified by the field amplitudes participating in this cubic term. For self-phase modulation (SPM), all three fields belong to the channel of interest; for cross-phase modulation (CPM), two fields belong to a different channel; and for four-wave mixing (FWM), all three amplitudes belong to other channels. Of these, FWM gives rise to additive noise to the channel of interest but is strongly suppressed by dispersion and will be omitted from the present considerations for simplicity. Its effects can be incorporated by including an additive term in the model below, and we comment on this at a later stage. We also neglect SPM, as these effects are deterministic for the given channel and could be reduced using nonlinear precompensation. Finally, we are left with CPM, which appears to be the principal source of nonlinear capacity impairment in the multi-user case for realistic parameter ranges. It causes multiplicative noise, which gives rise to qualitatively new effects and severe impairments in the channel capacity compared to additive noise. When channels are so close as to have almost overlapping frequency components, the sharp distinction between CPM and FWM is lost, owing to non-phase-matched terms that cannot be simply categorized. However, the distinction between multiplicative and additive noise can still be made, and here we group all multiplicative noise components (that is, those involving an amplitude from the channel of interest) under CPM.

We note that although CPM arises form a deterministic propagation equation of the full electric field, owing to the multi-user nature of WDM it nevertheless impairs the capacity; this effect is analogous to multi-user interference in wireless communication systems, except that in the present case, propagation nonlinearities cause users to interfere even though they have non-overlapping frequency bands.

We model the propagation channel in the presence of CPM by means of a linear Schrödinger equation with a random potential

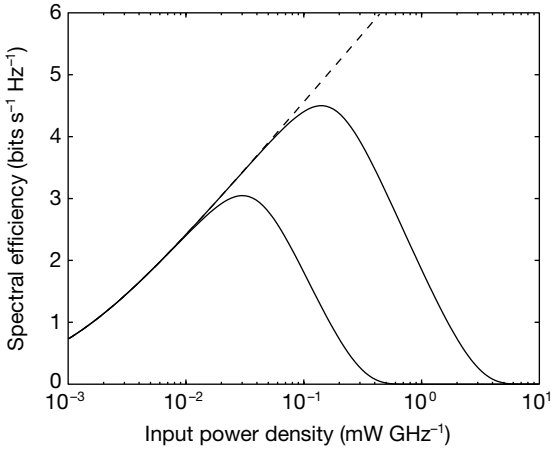

Figure 1 Spectral efficiencies. The curves represent lower bounds to the spectral efficiency for a homogenous length of fibre for a multi-user WDM system, given analytically by equation (2). Although the curves represent lower bounds, we argue in the text that the true capacity shows the same qualitative non-monotonic behaviour with respect to input signal powers. The spectral efficiencies displayed in the figure correspond to the capacity per unit bandwidth, $C' = C/(\eta_c \delta\nu)$. Here $\delta\nu$ includes both the channel bandwidths and the inter-channel spacing. The parameters used for the figure are $n_c = 100$, $L_{\mathrm{eff}} = 100$ km, $D = 20\,\mathrm{ps\,nm^{-1}\,km^{-1}}$, $\delta\nu = 1.5B$ where $B = 10$ GHz is the individual channel width. The two continuous curves correspond to $\gamma = 1\,\mathrm{W^{-1}\,km^{-1}}$ and $\gamma = 0.1\,\mathrm{W^{-1}\,km^{-1}}$. The lower curve corresponding to $\gamma = 1$. The spontaneous noise strength I_n is computed for the formula $I_n = aGh\nu Bn_s$ as explained in the text, with $a = 2$, $G = 1{,}000$, $\nu = 200$ THz. The dashed curve represents the spectral efficiencies of the corresponding linear channels given by $\gamma = 0$.

fluctuating both in space and time. This is easily justified, starting from the nonlinear Schrödinger equation description commonly used to describe light propagation in single-mode optical fibres[4]. If only CPM effects are retained, the propagation equation for the field amplitude E_i in channel i is given by:

$$i\partial_z E_i = \frac{\beta}{2}\partial_t^2 E_i + V(z,t)E_i \qquad (1)$$

where $V(z,t) = -2\gamma\Sigma_{j\neq i}|E_j(z,t)|^2$. Here β is the dispersion coefficient, t is time, z measures distance along the fibre, and ∂_z and ∂_t are partial derivatives with respect to z and t. Because independent streams of information are transmitted in the channels $j \neq i$, $V(z,t)$ appears as a random noise term to the channel i. We note that the nonlinear propagation equation has now been reduced to a linear Schrödinger equation with a stochastic potential, so that the nonlinear channel has become a channel with multiplicative noise. We now need an adequate model for the stochastic properties of $V(z,t)$. If the dispersion is substantial, we propose that $V(z,t)$ may be approximated by a gaussian stochastic process that is short-range-correlated in both space and time. As V is obtained by adding a large number of different channels, each of which is short-range-correlated in time ($\tau \approx 1/B$, where B is the channel bandwidth), we can expect V to have a correlation time of approximately $1/B$. Dispersion causes the channels to travel at different speeds, thus causing V to be short-range-correlated in space as well, with a correlation length related to the dispersion length. Because V is a sum of intensities, it has a non-zero mean, so we define $\delta V(z,t) = V(z,t) - \langle V\rangle$, where $\langle V\rangle$ denotes the average value of V. Removing a constant for the potential causes an overall phase shift independent of space and time, which is irrelevant to the present considerations.

The parameter of interest in the following is the integrated strength of the fluctuating field, $\eta = \int dz\langle\delta V(z,0)\delta V(0,0)\rangle$. In order to estimate η, we consider a simplified propagation model for the channels other than the one of interest, in which nonlinearities are neglected, and stochastic bit streams at the inputs to the channels are propagated forward with constant group velocities. The group velocity difference between two channels separated by a spacing $\Delta\lambda$ is $D\Delta\lambda$. In this model with n_c other channels evenly spaced by $\Delta\lambda$ around the channel of interest, each with intensity I and bandwidth B, we obtain $\eta = 2\ln(n_c/2)(\gamma I)^2/(BD\Delta\lambda)$. Here D is the dispersion parameter $D = -2\pi c\beta/\lambda^2$. Although this is a simplified model for the other channels, numerical simulations of propagation, including the nonlinearities and dispersion for the side channels, show that the estimate of η is accurate.

We note that the denominator in the expression of η is the inverse of the dispersion length L_D for the given channel spacing. This form for η follows from assuming that $L_{eff} \gg L_D$, because in this limit the integral defining η is cut off by L_D. If, on the other hand, $L_{eff} \leqslant L_D$, the integral would be cut off by L_{eff}, so that one would have to replace L_D by L_{eff} in the equation for η. Dispersion causes channels at spacing $\Delta\lambda_j$ to be suppressed proportionately to $1/(\Delta\lambda_j) \propto 1/j$, which leads to the logarithmic factor after summation.

The electric field evolution is given in terms of a propagator $U(t,t';L)$, obtained by integrating the stochastic Schrödinger equation. We model the amplifier noise as an additive term with strength I_n as defined earlier. The channel is specified in terms of a relation between the input and output electric field amplitudes, $E_{out}(t) = \int dt' U(t,t';L)E_{in}(t') + n(t)$. U is stochastic, so, owing to the underlying stochasticity of $V(z,t)$, the model corresponds to a channel with multiplicative noise. An exact capacity computation is still intractable, but an analytic lower bound may now be obtained, based on the following information theoretic result (E. Telatar, personal communications): the capacity C' of a channel with input X and output Y related by a conditional distribution $p(Y|X)$ and an input power constraint $E(||X||^2) = P$ satisfies the inequalities $C' = \max_{p(X)} I(X,Y) \geqslant I(X_G,Y) \geqslant I(X_G,Y_G)$. Here $I(X_G,Y)$ is the mutual information when $p(X)$ is chosen to be $p_G(X)$, a gaussian satisfying the power constraint; $I(X_G,Y_G)$ is the mutual information of a pair (X_G,Y_G) with the same covariance matrix as the pair (X_G,Y). The first inequality is trivial, as $p_G(X)$ is not necessarily the optimal input distribution. A proof of the second inequality is outlined in the Methods section.

The quantity $I(X_G,Y_G)$ may be computed from the correlators $\langle E_{in}(t)E_{in}^*(t')\rangle$, $\langle E_{out}(t)E_{out}^*(t')\rangle$ and $\langle E_{out}(t)E_{in}^*(t')\rangle$. The first is defined *a priori* through the assumption of band-limited gaussian white noise input with a power constraint. This is important for the application of the result above which requires a gaussian distribution for X. The second follows from the first using the unitarity of U. The third correlator requires computation of the average propagator $\langle U\rangle$, where the average is over realizations of $V(z,t)$. For a guassian, delta-correlated V, we obtain $\langle U(t,t';L)\rangle = \exp(-\eta L/2)U_0(t-t';L)$ (see Methods), where U_0 is the propagator for $V = 0$. Assembling these results, we finally obtain an analytic expression for a lower-bound C_{LB} to the channel capacity of the stochastic Schrödinger equation model:

$$C_{LB} = n_c B\log_2\left(1 + \frac{e^{-(I/I_0)^2}I}{I_n + \left(1 - e^{-(I/I_0)^2}\right)I}\right) \qquad (2)$$

where I_0 is given by

$$I_0 = \sqrt{\frac{BD\Delta\lambda}{2\gamma^2\ln(n_c/2)L_{eff}}} \qquad (3)$$

The fundamental departure from a linear channel in the above capacity expression is the appearance of a nonlinear intensity scale I_0. For $B = 40\,\text{GHz}$, $D = 20\,\text{ps nm}^{-1}\,\text{km}^{-1}$, $\Delta\lambda = 1\,\text{nm}$, $\gamma = 1\,\text{W}^{-1}\,\text{km}^{-1}$, $n_c = 100$, and $L_{eff} \approx n_c/\alpha = 100\,\text{km}$, we get $I_0 = 32\,\text{mW}$. Examination of equation (3) shows that I_0 has reasonable dependence on all relevant parameters: namely, it increases with dispersion, the bandwidth and the channel spacing, but decreases with increasing system length and number of channels.

The reason for the non-monotonic behaviour of the capacity estimate is that if we consider any particular channel, the signal in the other channels appear as noise in the channel of interest, owing to the nonlinearities. This 'noise' power increases with the 'signal' strength, thus causing degradation of the capacity at large 'signal' strength. The behaviour of equation (2) is graphically illustrated in Fig. 1, where the spectral efficiency (bits transmitted per second per unit bandwidth) is shown as a function of input power. The peak capacity, achieved for an intensity $I_{max} \approx (I_0^2 I_n/2)^{1/3}$, is given approximately by $C_{max} \approx \frac{2}{3}n_c B\log_2(2I_0/I_n)$.

We note that at large intensities, multiplicative noise causes an exponential attenuation of the effective signal power, which is why it dominates over nonlinear additive noise: the latter would contribute an additive term to the denominator in equation (2) that would be cubic in intensity. At large intensities where this term is important, the exponential in the numerator arising from multiplicative noise dominates.

If the input intensity is kept fixed, the capacity bound declines exponentially with the system length, in contrast with the power-law decay for the linear propagation channel. This is as expected, because correlations of the electric field decay exponentially due to the fluctuating potential in equation (1). On the other hand, the maximal spectral efficiency given by C_{max} declines only logarithmically.

Finally, we present qualitative arguments as to why the single-user case is expected to show the same non-monotonicity of spectral efficiency with the input signal intensities. In the multi-user case, unknown information in other channels leads to multiplicative noise. In the single-user case, the cubic nonlinearity is a deterministic process that would not by itself degrade channel capacity

except to a small extent through loss of power out of band. However, noise photons injected by the amplifiers and random photon deletion due to absorption cause the propagating field to acquire a stochastic component, which also leads to multiplicative noise effects through the nonlinear term. This leads us to believe that the single-user case will qualitatively exhibit the same decline in spectral efficiency with intensity as the multi-user case. The same qualitative arguments apply to interposing optical phase conjugation elements for nonlinear compensation; fibre absorption and amplifier noise can still be shown to cause multiplicative noise through the cubic term. It would be incorrect to conclude that nonlinearities must always impair capacity: signal regenerators are an obvious conter-example. However, the fundamental insight in the current work is that in nonlinear propagation channels, qualitatively new phenomena that arise from multiplicative noise effects can severely degrade capacity. □

Methods

Gaussian bound to the channel capacity

Proof of the inequality $I(X_G, Y) \geqslant I(X_G, Y_G)$: define $p(X, Y)$ as the product $p_G(X)p(Y|X)$, and $p_G(X, Y)$ to be the joint gaussian distribution having the same second moments as $p(X, Y)$. Also define $p_G(Y)$ to be the corresponding marginal of $p_G(X, Y)$.

$$I(X_G, Y) = \int dX dY p(X, Y) \log\left(\frac{p(X, Y)}{p_G(X)p(Y)}\right) \quad (4)$$

$$= \int dX dY p(X, Y)\left[\log\left(\frac{p_G(X, Y)}{p_G(X)p_G(Y)}\right) - \log\left(\frac{p_G(X, Y)p_G(Y)}{p(X, Y)p_G(X)}\right)\right] \quad (5)$$

As $p(X, Y)$ and $p_G(X, Y)$ share second moments, the first term on the right-hand side is $I(X_G, Y_G)$. The second term may be simplified using the convexity of the logarithm, $\langle\log(f)\rangle \leqslant \log(\langle f\rangle)$ to obtain

$$I(X_G, Y) \geqslant I(X_G, Y_G) - \log\left[\int dX dY p_G(X, Y)\frac{p(Y)}{p_G(Y)}\right] \quad (6)$$

$$\geqslant I(X_G, Y_G). \quad (7)$$

The second inequality follows by first performing the integral over X, and noting that $\log(\int dY p(Y)) = \log(1) = 0$.

Derivation of the average propagator $\langle U\rangle$

This can be done by resumming the perturbation series exactly for $\langle U\rangle$, for delta-correlated $V(z, t)$. Alternatively, using path integrals[7], $\langle U(t, t'; L)\rangle = U_0(t - t'; L)\langle\langle\exp(i\int_0^L dz V(z, t(z)))\rangle\rangle$, where the average is taken over V as well as over paths $t(z)$ satisfying $t(0) = t$, $t(L) = t'$. The result in the text follows by performing the gaussian average over V. Because $\phi = \int_0^L dz V(z, t(z))$ is a linear combination of gaussian variables, it is also gaussian-distributed and satisfies $\langle\exp(i\phi)\rangle = \exp(-\langle\phi^2\rangle/2)$. The result follows by noting that for delta-correlated V, $\langle\phi^2\rangle$ is a constant given by ηL. The delta correlations need to be treated carefully; this can be done by smearing the delta functions slightly and leads to the definition of η given earlier in the text.

Received 13 November 2000; accepted 19 April 2001.

1. Shannon, C. E. A mathematical theory of communications. *Bell Syst. Tech. J.* **27,** 379–423, 623–656 (1948).
2. Biglieri, E., Proakis, J. & Shamai, S. Fading channels: Information-theoretic and communications aspects. *Inform. Theory Trans.* **44,** 2619–2692 (1998).
3. Kogelnik, H. High-capacity optical communication. *IEEE Sel. Topics Quant. Elec.* **6**(6), 1279 (2000).
4. Agrawal, G. P. *Nonlinear Fiber Optics* (Academic, San Diego, 1995).
5. Desurvire, E. *Erbium Doped Fibre Amplifiers* 69 (Wiley, New York, 1994).
6. Cover, T. M. & Thomas, J. A. *Information Theory* 374–458 (Wiley, New York, 1991).
7. Feynman, R. P. & Hibbs, R. A. *Quantum Mechanics and Path Integrals* (McGraw-Hill, New York, 1963).

Acknowledgements

We gratefully acknowledge extensive discussions with E. Telatar, and also with A. Green, P. B. Littlewood, R. Slusher, A. Chraplyvy and G. Foschini. We thank M. Povinelli and L. Wegener for performing numerical and analytical computations to verify the considerations in this Letter, and D. R. Hamann and R. Slusher for careful readings of the manuscript.

Correspondence and requests for materials should be addressed to P.P.M. (e-mail: pmitra@bell-labs.com).

Control of conformational and interpolymer effects in conjugated polymers

J. Kim*† **& T. M. Swager**‡†

* *Department of Materials Science and Engineering,* † *Center for Materials Science and Engineering, and* ‡ *Department of Chemistry, Massachusetts Institute of Technology, Cambridge, Massachusetts 02139, USA*

The role of conjugated polymers in emerging electronic, sensor and display technologies is rapidly expanding. In spite of extensive investigations[1–11], the intrinsic spectroscopic properties of conjugated polymers in precise conformational and spatial arrangements have remained elusive. The difficulties of obtaining such information are endemic to polymers, which often resist assembly into single crystals or organized structures owing to entropic and polydispersity considerations. Here we show that the conformation of individual polymers and interpolymer interactions in conjugated polymers can be controlled through the use of designed surfactant poly(*p*-phenylene-ethynylene) Langmuir films. We show that by mechanically inducing reversible conformational changes of these Langmuir monolayers, we can obtain the precise interrelationship of the intrinsic optical properties of a conjugated polymer and a single chain's conformation and/or interpolymer interactions. This method for controlling the structure of conjugated polymers and establishing their intrinsic spectroscopic properties should permit a more comprehensive understanding of fluorescent conjugated materials.

We designed and synthesized (see Supplementary Information for details) four poly(*p*-phenylene-ethynylene) compounds (PPEs) using four surfactant 'building blocks' that display preferential orientations at the air–water interface. Unique combinations of these building blocks (A–D in Fig. 1) allow us to control an isolated polymer chain's conformation and interpolymer interactions. Building block A, with two *para*-hydrophobic dioctylamide groups, is expected to display a face-on structure, with its phenyl groups co-facial to the air–water interface[12,13]. B has two *para*-hydrophilic triethyleneoxide groups, and is also expected to prefer a face-on structure. The third building block, C, has one hydrophobic and one hydrophilic group *para* to each other, and is inclined towards an equilibrium edge-on structure with the π-plane normal to the interface. The last block, D, with two *ortho*-hydrophobic dodecyloxy groups, favours an edge-on structure. By design we have used these four building blocks to produce PPEs with precise structural features at the air–water interface. As we will show below, these polymers display one of three equilibrium organizations—face-on, alternating face-on and edge-on (zipper), or edge-on—depending upon the structure and surface pressure (Fig. 1).

Central to our analysis is the ability to switch between different structures, by applying mechanical force while monitoring the Langmuir monolayer's optical spectra. Figure 1 shows the chemical structures, conformations and spatial arrangements at the air–water interface of the PPEs. Our assignments of the conformations and spatial arrangements are based on a self-consistent analysis of the pressure–area (P–A) isotherms (Fig. 2a), *in situ* ultraviolet–visible (UV–vis.) and fluorescence spectroscopy (Fig. 3), and molecular modelling (Fig. 2b). Polymer **1** favours the face-on structure with a large extrapolated area per repeating unit of 240 Å^2. As the monolayer is compressed, the surface pressure increases until the monolayer folds into multilayers at 30 mN m^{-1} with an area per repeating unit of 130 Å^2. Molecular modelling predicts a repeating unit area of 126 Å^2 when **1** is highly compressed in the face-on structure (Fig. 2b). The wavelength of maximum